

OccGS: Zero-shot 3D Occupancy Reconstruction with Semantic and Geometric-Aware Gaussian Splatting

Xiaoyu Zhou¹ Jingqi Wang¹ Yongtao Wang^{1*} Yufei Wei² Nan Dong² Ming-Hsuan Yang³

¹Wangxuan Institute of Computer Technology, Peking University

²Chongqing Changan Automobile Co., Ltd ³University of California, Merced

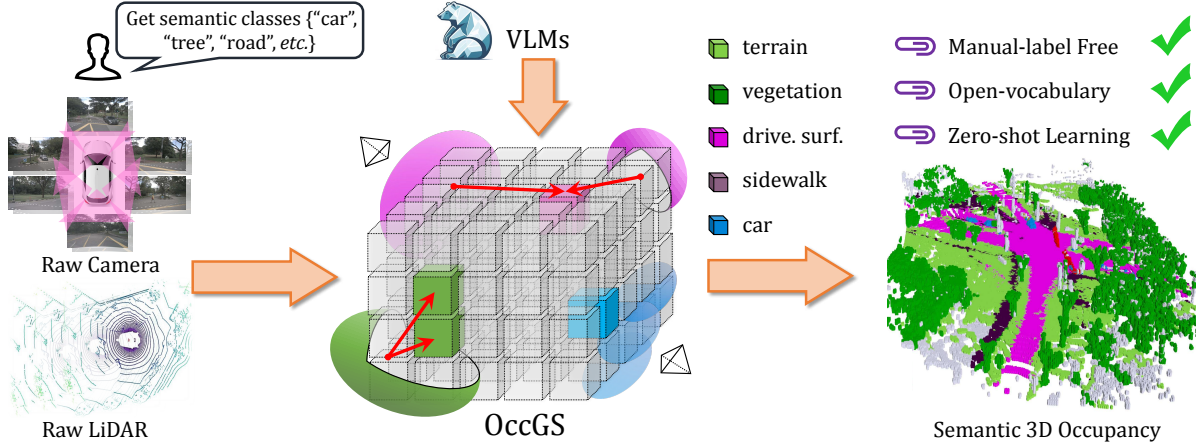


Figure 1. **OccGS** reconstructs the semantic 3D occupancy of the scene from multimodal sensor data, using Semantic and Geometric-Aware Gaussian Splatting in combination with vision-language models (VLMs), without requiring any manual annotations. **OccGS** enables: 1) label-free training, 2) open-vocabulary semantic occupancy estimation, and 3) zero-shot cross-dataset scene-aware learning.

Abstract

Obtaining semantic 3D occupancy from raw sensor data without manual annotations remains an essential yet challenging task. While prior works have approached this as a perception prediction problem, we formulate it as scene-aware 3D occupancy reconstruction with geometry and semantics. In this work, we propose *OccGS*, a novel 3D **O**ccupancy reconstruction framework utilizing **S**emantic and **G**eometric-Aware **G**aussian Splatting in a zero-shot manner. Leveraging semantics extracted from vision-language models and geometry guided by LiDAR points, *OccGS* constructs **S**emantic and **G**eometric-Aware **G**aussians from raw multisensor data. We also develop a cumulative Gaussian-to-3D voxel splatting method for reconstructing occupancy from the Gaussians. *OccGS* performs favorably against self-supervised methods in occupancy prediction, achieving comparable performance to fully supervised approaches and achieving state-of-the-art performance on zero-shot semantic 3D occupancy estimation.

*Corresponding author.

1. Introduction

The perception and construction of 3D scenes have long been resource-intensive tasks, demanding extensive manual annotations and significant training costs. Concurrently, emerging as a general description of the physical world, 3D occupancy has garnered notable attention in autonomous driving [51, 53, 55] and embodied intelligence [6, 39, 40]. By jointly learning geometry and semantics, 3D occupancy shows great promise to facilitate holistic scene understanding and irregular object detection. Despite its potential in 3D perception, constructing high-fidelity semantic 3D occupancy from raw sensor data (collected by mobile driving platforms) with limited observations remains a challenge.

To obtain scene occupancy, existing methods [16, 27, 28, 36, 60, 64] typically adopt training-based approaches, learning the occupancy status of 3D voxels from a large set of scenes with manually labeled annotations. Despite promising results, these algorithms depend heavily on pre-annotated dense ground truth (e.g., 3D occupancy GT), which is time-consuming to produce and prone to subjective bias. Recent self-supervised occupancy estimation methods [3, 12, 13, 17, 66] utilize vision-centric 2D images or

annotations to alleviate reliance on 3D labels. Nonetheless, these approaches encounter substantial challenges in preserving the completeness and consistency of scene occupancy, as their lack of awareness of complex scene geometry results in considerable prediction errors. The methods above struggle to achieve open-vocabulary occupancy and lack generalization across datasets and scenes. Their high computational and storage costs due to dense representations, stemming from dense representations and sampling, limit their applicability to diverse downstream tasks.

In this paper, we present OccGS, an efficient and effective framework for semantic 3D occupancy reconstruction, enabling open-vocabulary occupancy estimation and generalizable zero-shot optimization. We formulate scene occupancy prediction as the reconstruction of geometric and semantic representation. Based on this, we introduce Semantic and Geometric-Aware Gaussians (SGAG). Benefiting from the semantic information provided by vision-language models (VLMs) and the geometric priors guided by LiDAR, OccGS facilitates high-quality understanding and reconstruction of the holistic scene. In addition, we introduce dynamic object clustering to identify moving instances within the scene and enhance their geometric integrity. As such, OccGS reconstructs the scene’s semantic occupancy from SGAG with a cumulative Gaussian-to-3D voxel splatting. Extensive experiments show that OccGS outperforms self-supervised methods and achieves competitive performance compared to fully supervised approaches using 3D annotations. Our method further exhibits excellent open-vocabulary and zero-shot generalization capabilities, as evidenced by cross-dataset experiments. Our main contributions include:

- We propose formulating the scene occupancy estimation task as the reconstruction based on geometric and semantic representations, demonstrating strong open-vocabulary and zero-shot generalization capabilities.
- We devise an enhanced semantic and geometric-aware Gaussians representation, integrating semantic guidance from VLMs and multimodal geometric priors, while obtaining high-quality occupancy at low cost via the proposed cumulative Gaussian-to-3D voxel splatting.
- OccGS achieves a balanced trade-off between accuracy, efficiency, and flexibility in 3D occupancy reconstruction, surpassing or matching the performance of existing self-supervised and fully supervised approaches.

2. Related Work

Semantic 3D Occupancy Prediction. Semantic 3D occupancy prediction [50, 54, 68] aims to estimate the occupancy states and semantics of complex scenes, which is crucial for 3D perception and planning. Based on the work on 3D Bird’s eye view (BEV) perception, numerous methods [16, 27, 28, 36, 44, 64, 68] generate volume features

from multi-view images and predict 3D occupancy with a prediction head. Despite the promising performance of these fully supervised methods, they are limited to predicting occupancy at a fixed voxel resolution, falling short of attaining finer-grained, multi-resolution scene understanding. Furthermore, these methods heavily rely on voxel-level 3D labels at each stage of training, such as 3D occupancy ground truth. Manually annotating these labels is time-consuming, labor-intensive, and prone to ambiguity due to subjective bias [37].

Recent advances in self-supervised methods [2, 3, 12, 17, 66] for estimating 3D occupancy from 2D supervision have reduced reliance on costly annotations. Employing neural rendering techniques [34, 48] (*e.g.*, NeRF) to align multi-view image features with 3D volume features, these approaches commonly use pixel-level 2D labels (from 3D projections [37] or open-vocabulary models [52]) to train occupancy prediction networks.

However, these methods struggle to accurately estimate the holistic semantic occupancy of complex scenes. The 2D-to-3D projection introduces ambiguity and illusion, causing misalignment in scene geometry and temporal inconsistency. Additionally, training-based approaches tend to overfit specific sensor parameters and dataset occupancy distributions, limiting cross-dataset and scene-aware generalization capabilities.

To address these limitations, we formulate the scene semantic occupancy problem from the perspective of reconstruction. We propose a fully reconstruction-based occupancy estimation framework that requires no manual 2D/3D annotations, achieving high-precision open-vocabulary retrieval, zero-shot learning, and cross-dataset generalization.

Scene Representation and Reconstruction. Constructing an efficient representation is the core to obtaining complete scene occupancy. Dense voxel-based methods [4, 7, 23, 24] assign each voxel a feature vector, inevitably suffering from high computational cost due to redundant grids. As a compressed representation, BEV [5, 14, 26, 33] schemes encode 3D information in the ground plane. Lacking vertical dimension information, BEV fails to estimate the diverse 3D geometry using flattened vectors. To overcome this limitation, recent methods [16, 57, 59] add two additional planes to form a tri-perspective view (TPV), yet still leading to scene occlusions and conflicts at the horizontal scale.

By implicitly modeling 3D space, Neural radiance field (NeRF) [34, 47] has been widely used for scene reconstruction. [13, 17, 37, 66] build a NeRF-style 3D volume and estimate scene occupancy from it. However, the continuous implicit neural fields pose a significant challenge in effectively learning the geometry of complex dynamic scenes through pixel-level supervision. Moreover, the dense sampling operation introduces redundant and costly memory.

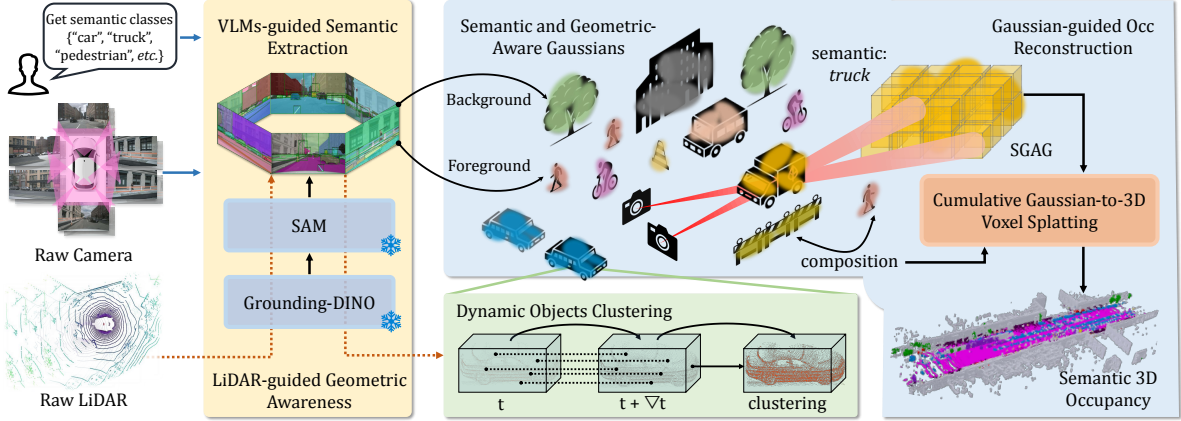


Figure 2. **Overall pipeline of our method.** Given arbitrary semantic prompts, OccGS reconstructs the scene and generates semantic 3D occupancy from unlabeled multi-sensor data, including multi-camera images and LiDAR scans. OccGS first extracts semantic information from images using VLMs and aligns it with LiDAR points in 3D space. The scene is then reconstructed based on the proposed Semantic and Geometric-Aware Gaussians (SGAG), which decouple the foreground and background while clustering dynamic objects. Finally, we generate the semantic 3D occupancy through cumulative Gaussian-to-3D voxel splatting, guided by the composed SGAG.

Most recently, 3D Gaussian splatting (3DGS) [20, 38, 65] has demonstrated its powerful capability in reconstruction and rendering, even for driving scenes [11, 49, 75]. However, only a few methods have leveraged 3DGS for semantic occupancy estimation. GaussianFormer [18] uses 3D ground truth supervision with sparse convolution and cross-attention to transform 2D into 3DGS, while GaussianOcc [12] adopts a self-supervised approach, treating each vertex as a Gaussian. However, assigning a 3D Gaussian to each vertex not only results in a dramatic increase in computational cost, but also limits the ability of 3DGS to efficiently model scenes with varying scales.

In contrast to prior art, we enhance 3DGS with geometric and semantic awareness by proposing Semantic and Geometric-Aware Gaussians. We further design a cumulative Gaussian-to-3D voxel splatting that reconstructs dense semantic voxels from sparse representations, enabling efficient and cost-effective semantic occupancy acquisition.

Vision Foundation Models for 3D Occupancy. Vision-language Models (VLMs) [22, 58] have shown promising results and generalization ability across various visual tasks. However, their application to 3D occupancy has received limited attention. Unlike direct training with 3D annotations, existing foundational vision models [19, 21, 30, 42] are primarily trained on 2D images, which may challenge the consistency of 3D occupancy across different cameras and frames. In this work, we explore the potential of applying VLMs [21, 30, 42] to occupancy estimation and utilize them for open-vocabulary semantic extraction. To mitigate 3D semantic inconsistencies caused by VLMs [15, 61, 67], we incorporate multimodal geometric priors and an improved 3DGS representation.

3. Method

Given multi-view images $I = \{I_t^1, I_t^2, \dots, I_t^S\}$, corresponding multi-frame LiDAR sweeps L_t , and text prompts of arbitrary semantics C , OccGS reconstructs the complete semantic 3D occupancy of the scene all at once, without using any manual annotations. Figure 2 illustrates the overall framework. Starting with the construction of Semantic and Geometric-Aware Gaussians (Section 3.1), we incorporate VLMs along with sparse LiDAR points to provide semantic and geometric prior constraints. During this process, dynamic objects are clustered at the instance level to more effectively capture the motion states of dynamic regions (Section 3.1). We then design a Gaussian-guided Occupancy (Occ) reconstruction to efficiently obtain the scene’s semantic 3D occupancy (Section 3.2).

3.1. Semantic and Geometric-Aware Gaussians

Open-world driving scenes encompass intricate geometry, diverse semantics, and numerous dynamic objects. To achieve comprehensive scene understanding under such complex conditions, we propose Semantic and Geometric-Aware Gaussians (SGAG) as an intermediate representation that bridges raw sensor data with semantic 3D occupancy.

SGAG enhances 3DGS [20] in three aspects: incorporating VLMs-guided semantic attributes, leveraging geometric priors from visual semantics and LiDAR points, and applying flow clustering for dynamic objects. Each Gaussian ellipsoid is characterized by a centroid o , a scale factor s , a rotational quaternion q , an opacity α , a semantic probability γ , a dynamic vector v indicating the motion state of the corresponding objects, and a time sequence token t . The enhanced 3DGS enables each Gaussian to incorporate semantic, geometric, and dynamic awareness, thus facilitating

a more accurate reconstruction of semantic occupancy.

VLMs-guided semantic awareness. To enable open-vocabulary semantic reconstruction in 3D scenes, we first deploy VLMs to automatically extract 2D semantic priors from multi-view images and align these priors with the scene geometry in 3D space using multimodal data. Taking multi-view images as input, we combine Grounding-DINO [30] with SAM2 [41] to extract the segmentation binary mask M corresponding to the semantic prompts, and generate a semantic label ϕ for each pixel. The blended semantic labels of Gaussians can be obtained via α -blending:

$$\Gamma_i = \sum_{i=1}^N \text{softmax}(\gamma_i) \alpha_i \prod_{j=1}^{i-1} (1 - \alpha_j), \quad (1)$$

where Γ_i is the rendered semantic for each pixel, weighted by the Gaussian’s semantic probability γ and opacity α . We leverage cross-entropy loss to the rendered semantics:

$$L_{sem} = - \sum_{i=1}^Q \sum_{k=1}^K \gamma_{i,k} \log \phi_{i,k}, \quad (2)$$

where $\phi_{i,k}$ is the pixel-level semantic label from VLMs.

LiDAR-guided geometric awareness. We leverage sparse, unlabeled LiDAR points to provide geometric priors for the Gaussians and to initially align the scene semantics. Similar to [71, 72], a point $p_{i,t}$ in the LiDAR sweep L_t is projected onto the frame I_t , and its initial semantic label can be obtained by $K^{-1}[R^\top \phi_{x,y,t} + T]$, where (K, R, T) are the corresponding camera parameters and homogenous transformation matrix, and ϕ is the pixel-level semantic label. We aggregate the multi-frame of LiDAR points over time and compute the anchor centers $p_c = (x_c^i, y_c^i, z_c^i)$ for different semantics to initialize the Gaussians in SGAG. We then implement a geometry-aware loss to enforce the alignment of Gaussian ellipsoid distributions with the geometric priors of their corresponding semantic regions:

$$L_{geo} = - \sum_{c=1}^C \sum_{i=1}^M \frac{1}{\|o_c(i) - p_c(i)\|_2^2}, \quad (3)$$

where C denotes the number of semantic categories, M is the number of Gaussian ellipsoid centers within the anchor range, and o_i is the coordinate of the i -th Gaussian center.

Foreground and background decoupling. To balance reconstruction accuracy and efficiency, we ensure high-quality geometry in detailed regions while reducing computation for large-scale areas by decoupling foreground and background elements based on their geometric and semantic characteristics. For small objects in the scene (*e.g.*, cones, ashbins), we use dense bilinear upsampling and constrain the scale s of the corresponding Gaussian ellipsoids

within a smaller optimization range. In contrast, for larger background elements such as buildings, we expand the scale range of the SGAG to efficiently represent large-scale areas with sparser Gaussians. This approach enables SGAG to better capture the geometry of different semantic objects and reconstruct them at varying resolutions. Finally, the Gaussians representing the foreground objects and background are composed and jointly optimized.

Dynamic objects clustering. Reconstructing dynamic objects is essential for driving scenes understanding, but separating them without dynamic annotations remains challenging. To address this, we combine dynamic semantics with self-estimated scene flow to identify and cluster dynamic objects using Gaussians. Given the semantics of movable objects (*e.g.*, vehicles, pedestrians, *etc.*), we first extract the corresponding foreground regions from adjacent frame images. Motivated by [9, 10, 29], we search for Gaussian clusters of movable objects at time t_i and pair them with neighboring clusters at time $t_{i\pm 1}$. Since movable objects may be stationary in the current frame, we define a dynamic indicator function between paired clusters to determine whether an object is in motion:

$$\mathbb{1}(D) = \rho - \frac{1}{m} \sum_{i=1}^m \sum_{j=1}^n \|o_{t+1}^i - o_t^j\|_2, \quad (4)$$

where D is the average distance between paired Gaussian clusters, ρ is the dynamic threshold, m and n denote the number of Gaussian ellipsoids. The centroid position at the i -th frame is denoted by o_i . A Gaussian cluster is considered a dynamic object and assigned a value of $v = 1$ if $\mathbb{1}(D) > 0$. Subsequently, we aggregate all temporally paired Gaussian clusters based on geometry and motion. For each instance sharing the same semantic index γ_i , we track the corresponding Gaussians ($v = 1$) and consolidate them into a unified coordinate system using ego-motion transformations at each time step. The Gaussians of dynamic objects are then merged with the background, forming a complete Gaussian representation of the scene.

3.2. Gaussian-guided Occ Reconstruction

Different from existing methods [12, 31], we do not establish a one-to-one correspondence between Gaussians and occupancy. Instead, we exploit the sparsity of Gaussians from SGAG to reduce optimization costs, while enabling a more continuous and detailed understanding of both semantics and geometry. To this end, we propose a cumulative Gaussian-to-3D voxel splatting technique for gaussian-guided occupancy reconstruction.

First, the space occupied by each Gaussian cannot be simply calculated by its centroid position $\{o_x, o_y, o_z\}$ due to the variations in anisotropic shape and spatial overlap. Thus, we estimate the occupied range of each Gaussian by

Table 1. **3D occupancy estimation on Occ3D-nuScenes [50]**. 3D Occ refers to annotated occupancy GT, LiDAR denotes manually labeled semantic point clouds, 2D represents 2D semantic labels derived from 3D, and N/A indicates the absence of manual annotations. “cons. veh.” and “drive. surf.” stand for construction vehicles and driveable surfaces, respectively. TPVFormer* is trained with labeled LiDAR. OccGS-Z is the version of OccGS without using any manual labels, while OccGS-S adopts 2D semantic annotations from [37]. The intersection over union (IoU) and mean IoU of semantic classes (mIoU) are calculated over all voxels.

Method	Supervision	IoU ↑	mIoU ↑	barrier	bicycle	bus	car	cons. veh.	motorcycle	pedestrian	traffic cone	trailer	truck	drive. surf.	sidewalk	terrain	manmade	vegetation
				■	■	■	■	■	■	■	■	■	■	■	■	■	■	■
MonoScene [4]	3D Occ	-	6.33	7.23	4.26	4.93	9.38	5.67	3.98	3.01	5.90	4.45	7.17	14.91	7.92	7.43	1.01	7.65
BEVStereo [25]	3D Occ	-	25.47	38.41	7.88	38.7	41.2	17.56	17.33	14.69	10.31	16.84	29.62	54.08	32.68	26.54	18.74	17.49
BEVFormer [27]	3D Occ	-	28.19	37.83	17.87	40.44	42.43	7.36	23.88	21.81	20.98	22.38	30.70	55.35	36.00	28.06	20.04	17.69
OccFormer [68]	3D Occ	-	22.40	30.29	12.32	34.40	39.17	14.44	16.45	17.22	9.27	13.90	26.36	50.99	34.66	22.73	6.76	6.97
TPVFormer [59]	3D Occ	-	28.70	38.90	13.67	40.78	45.90	17.23	19.99	18.85	14.30	26.69	34.17	55.65	37.55	30.70	19.40	16.78
TPVFormer* [59]	LiDAR	17.20	13.89	14.82	9.43	21.30	16.79	14.51	13.82	11.24	5.35	16.17	19.70	10.81	9.52	11.24	16.57	17.03
FB-Occ [28]	3D Occ	77.45	28.87	40.91	21.22	39.17	40.80	20.61	23.78	23.62	25.03	16.61	26.35	59.42	31.43	29.02	16.67	18.42
CTF-Occ [50]	3D Occ	-	29.54	39.33	20.56	38.29	42.24	16.93	24.52	22.72	21.05	22.98	31.11	53.33	37.98	33.23	20.79	18.00
GaussianFormer [18]	3D Occ	-	18.82	19.52	11.26	26.11	29.78	10.47	13.83	12.58	8.67	12.74	21.57	39.63	24.46	22.99	9.59	19.12
SurroundOcc [56]	3D Occ	-	20.07	20.59	11.68	28.06	30.86	10.70	15.14	14.09	12.06	14.38	22.26	37.29	24.49	22.77	14.89	21.86
RenderOcc [37]	2D	-	24.52	27.56	14.36	19.91	20.56	11.96	12.42	12.14	14.34	20.81	18.94	68.85	42.01	43.94	17.36	22.61
SimpleOcc [13]	2D	-	7.99	0.67	1.18	3.21	7.63	1.02	0.26	1.80	0.26	1.07	2.81	40.44	18.30	17.01	13.42	10.84
OccGS-S	2D	83.10	36.99	31.67	19.18	20.42	32.25	24.28	14.20	23.98	39.53	18.05	29.91	62.05	40.48	43.32	72.33	83.26
SelfOcc [17]	N/A	45.01	10.57	0.21	0.73	5.50	12.52	0.10	0.82	2.09	0.00	0.00	8.31	55.53	26.30	26.62	14.21	5.64
OccNeRF [66]	N/A	53.57	10.81	0.83	0.82	5.13	12.49	3.50	0.23	3.10	1.84	0.52	3.90	52.62	20.81	24.75	18.45	13.19
GaussianOcc [12]	N/A	-	11.26	1.79	5.82	14.58	13.55	1.30	2.82	7.95	9.76	0.56	9.61	44.59	20.10	17.58	8.61	10.29
LangOcc [2]	N/A	-	12.05	2.73	7.21	5.78	13.92	0.51	10.80	6.42	8.67	3.24	11.02	42.10	12.44	27.17	14.13	14.55
VEON [73]	N/A	-	13.98	4.80	2.70	14.70	10.90	11.00	3.80	4.70	4.00	5.30	9.60	46.50	21.10	22.10	24.80	23.70
OccGS-Z	N/A	83.82	30.26	13.50	20.10	18.63	33.79	12.18	17.54	30.18	28.58	2.18	23.75	62.67	29.89	36.81	55.24	68.83

considering the distance from the nearest tangent surface of the Gaussian ellipsoid to the voxel as:

$$d = o_z - \frac{\eta^{-1} \Sigma_{0,2}^{-1} (o_x - \kappa_x) + \eta^{-1} \Sigma_{1,2}^{-1} (o_y - \kappa_y)}{\Sigma_{2,2}^{-1}}, \quad (5)$$

where d is the occupied depth from the voxel to the Gaussian ellipsoid, η is the ray direction from the voxel center $k = (\kappa_x, \kappa_y, \kappa_z)$ to the Gaussian. Σ is the covariance matrix, with $\Sigma_{i,j}$ denoting the corresponding matrix elements. The Gaussian value $G(x)$ can be formulated as:

$$G(x) = e^{-\frac{1}{2}(\kappa - o)^\top \Sigma^{-1} (\kappa - o)}. \quad (6)$$

We then cumulatively splat SGAG Gaussians onto the voxel grid, with each voxel’s semantic label determined by weighting the occupied range and opacity from Gaussians:

$$F(o) = \sum_{i=1}^N d_i G(x_i) \alpha_i \text{softmax}(\gamma_i), \quad (7)$$

where d_i is the occupied depth of the Gaussian-to-3D voxel, treated as the splatting weight coefficient. α_i is the opacity, and $\text{softmax}(\gamma_i)$ computes the semantic probability.

We sort the semantic probabilities for each voxel and select the highest as the voxel’s final category. Additionally, we filter voxel positional noise using the k nearest neighbor algorithm, guided by semantic and geometric priors, to

prevent outliers from affecting the occupancy generation results. The Euclidean distance between queried semantic occupancy and corresponding semantic points is computed by:

$$\text{dist}(p_v, p_c) = \sqrt{\sum_i (p_v(i) - p_c(i))^2}, \quad (8)$$

where p_v is the center of the queried semantic occupancy and p_c is the anchor center with matching semantics. Outliers are rejected if their distance $\text{dist}(p_v, p_c)$ from the semantic cluster center exceeds a threshold τ_c , which varies depending on the semantic category.

4. Experiments

4.1. Datasets

Occ3D-nuScenes [50] is a large-scale 3D occupancy prediction benchmark, consisting of 600 scenes for training and 150 for evaluation. Each sample is collected using six surrounding cameras and a LiDAR, covering a range of [-40m, -40m, -1m, 40m, 40m, 5.4m] and a 0.4m voxel size. Although OccGS supports open-vocabulary semantic estimation at any voxel resolution, we follow the predefined semantic categories and sampling resolution for fair comparison. Similar to [66, 73], we evaluate our method on validation sets without considering the “other” and “other flat” classes, as open-vocabulary VLM models cannot recognize these ambiguous semantic categories.

Table 2. **Zero-shot cross dataset performance on SemanticKITTI [1]**. Nusc, other-veh. and moto-cyc. are short for Occ3D-nuScenes, other-vehicle, and motorcycles, respectively. All methods are trained on Occ3D-nuScenes and evaluated on SemanticKITTI. Novel class refers to unseen semantics in Nusc, while base class includes those seen during training. Metric mIoU-base denotes the mIoU computed solely on base classes.

Method	(a) Val: SemanticKITTI			(b) Novel Class						(c) Base Class										mIoU-base \uparrow		
	Training Set	IoU \uparrow	mIoU \uparrow	bicyclist	moto-cyc.	parking	fence	trunk	pole	traffic-sign	bicycle	car	other-veh.	motorcycle	pedestrian	truck	road	sidewalk	terrain		building	vegetation
TPVFormer [59]		2.29	0.78	0.0	0.0	0.0	0.0	0.0	0.0	0.0	0.58	2.30	1.56	0.23	1.70	1.43	2.55	0.82	0.34	0.74	1.84	1.28
TPVFormer* [59]		1.67	0.64	0.0	0.0	0.0	0.0	0.0	0.0	0.0	0.22	1.70	1.45	0.23	1.16	1.55	2.05	0.86	0.68	0.36	1.22	1.04
GaussianFormer [18]		3.44	1.13	0.0	0.0	0.0	0.0	0.0	0.0	0.0	0.12	3.69	0.30	0.46	0.67	1.57	9.01	1.06	2.04	0.36	1.18	1.85
OccNeRF [66]	Nusc	10.38	1.90	0.0	0.0	0.0	0.0	0.0	0.0	0.0	0.49	0.57	0.10	0.10	0.54	0.17	4.77	7.49	9.05	1.87	4.67	3.13
GaussianOcc [12]		11.10	2.99	0.0	0.0	0.0	0.0	0.0	0.0	0.0	1.26	5.33	1.09	0.77	1.63	0.83	26.55	4.88	5.76	1.58	4.14	4.89
OVO [46]		21.17	6.94	0.90	0.0	0.68	3.50	2.31	0.60	2.20	0.40	12.70	3.50	0.22	0.74	0.70	19.44	24.81	4.86	11.70	15.62	8.61
OccGS-Z		<u>49.98</u>	<u>15.97</u>	1.94	4.45	2.81	6.11	5.89	17.69	10.85	7.72	31.40	4.81	16.96	14.78	10.46	51.26	25.67	24.01	19.73	30.93	<u>21.61</u>

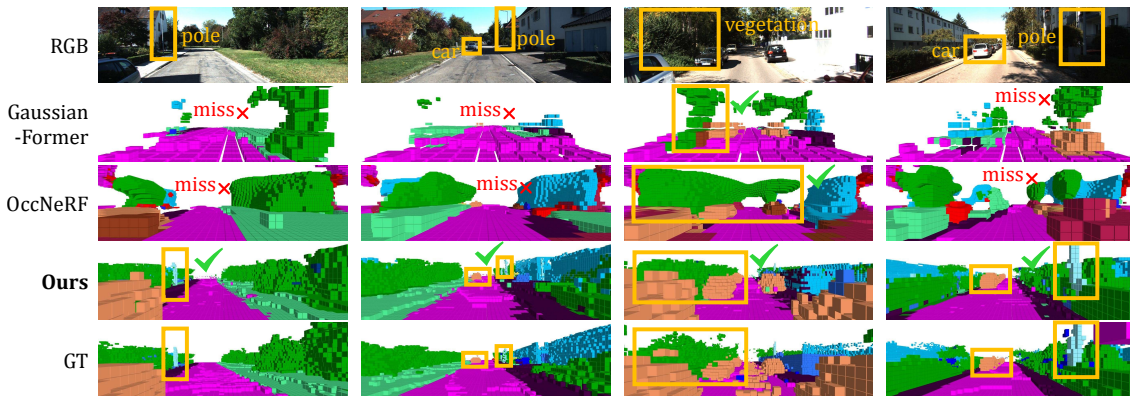


Figure 3. **Qualitative results of zero-shot validation on SemanticKITTI [1]**. OccGS achieves promising results in zero-shot cross dataset experiments, achieving high-quality semantic occupancy reconstruction of complex geometries and distant, fine objects.

SemanticKITTI [1] includes 22 forward driving scenes, where each sample covers a range of [0.0m, -25.6m, -2.0m, 51.2m, 25.6m, 4.4m] with 0.2m voxel size. SemanticKITTI provides 19 semantic categories, 7 unseen by Occ3D-nuScenes, as shown in Table 2. We employ SemanticKITTI to evaluate the model’s zero-shot performance and open-vocabulary occupancy estimation capabilities.

4.2. Implementation Details

We set the resolutions of images as 900×1600 for Occ3D-nuScenes and 370×1226 for SemanticKITTI. During optimization, we scale the image size to 225×400 and double it every 300 steps until reaching the original resolution. The hyperparameters ρ is set to 4. We use the AdamW optimizer for optimization with an initial learning rate of 0.005. The learning rate for the position parameters decays every 250 steps with a decay rate of 0.98. All experiments are carried out on 8 A100 GPUs.

4.3. Performance Evaluation and Analysis

We evaluate our method against the state-of-the-art (SOTA) approaches, including supervised methods with 3D Ground

Truth [4, 18, 25, 27, 28, 56, 59, 68], supervised methods with 2D Ground Truth [14, 37], and fully self-supervised methods without manual labels [2, 12, 17, 66, 73].

Supervised methods with 3D ground truth. Supervised Occ prediction approaches require supervision from costly 3D occupancy GT. In comparison, our method requires no manual annotations yet achieves competitive performance. Table 1 shows OccGS performs favorably against [4, 56, 68], which directly learn scene representations using voxels. The BEV-based approaches BEVFormer [27] and BEVStereo [25] achieve high prediction accuracy but lose 3D information due to the absence of height dimensions. OccGS outperforms TPVFormer [59] and FB-Occ [28], where the former enhances BEV with two vertical planes, and the latter combines BEV with voxels. OccGS also achieves results comparable to CTF-Occ [50]. Although both use LiDAR scans as input, our approach outperforms LiDAR-supervised TPVFormer* across all metrics. The Gaussian-based algorithm GaussianFormer [18] suffers from significant degradation, while our proposed SGAG representation achieves better robustness. Furthermore, the

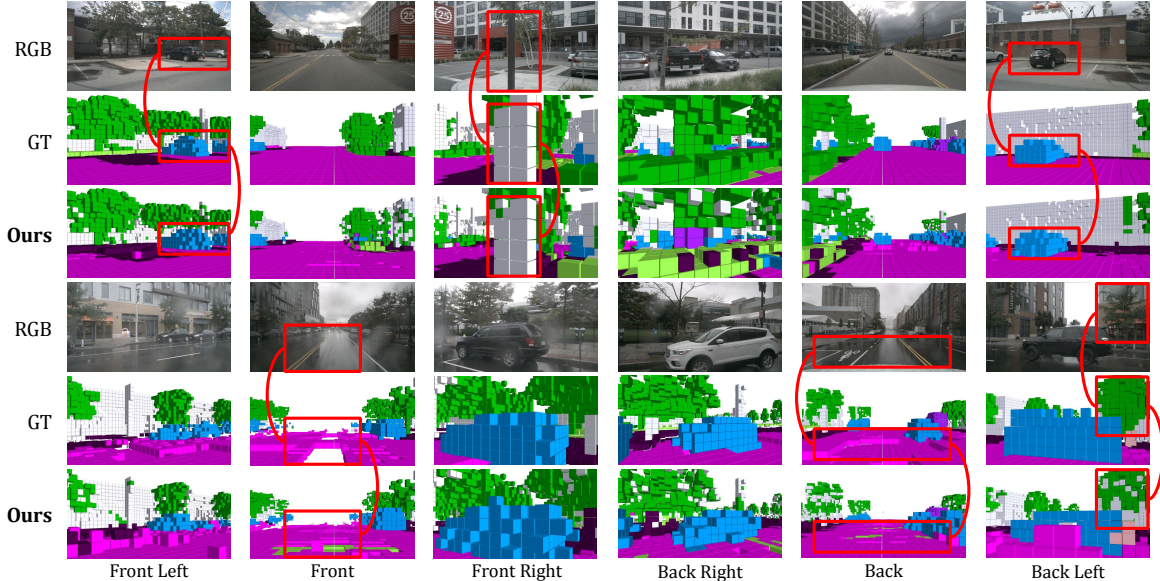


Figure 4. **Qualitative results of semantic occupancy reconstruction on Occ3D-nuScenes [50].** Our method enables high-quality reconstruction of semantic 3D occupancy in dynamic objects and complex scenes, even under extreme weather conditions.

above methods are limited to closed-vocabulary semantic occupancy prediction. In contrast, OccGS achieves a better trade-off between accuracy and generalization.

Supervised methods with 2D ground truth. Instead of using dense 3D ground truth, RenderOcc [37] and SimpleOcc [14] generate depth maps and 2D segmentations by projecting LiDAR points with 3D segmentation labels onto 2D images. In comparison, our method exhibits a better performance without using any manually labeled 2D ground truth (*i.e.*, OccGS-Z). For fair comparison, we substitute VLMs-guided semantic extraction with the 2D labels used in the aforementioned methods (*i.e.*, OccGS-S). Table 1 shows that by using 2D labels, OccGS achieves performance improvements. Despite potential semantic hallucinations from VLMs, OccGS alleviates this through multi-view optimization and 3D alignment, while still benefiting from manually labeled ground truth.

Fully self-supervised methods. We evaluate our method against fully self-supervised approaches that also do not require any manually labeled annotations. SimpleOcc [14] and OccNeRF [66] adopt the dense sampling and volume rendering of NeRF for self-supervised training. However, they lack awareness of scene geometry, facing challenges in complex driving scenes with intricate structures and various occlusions. OccGS performs well against LangOcc [2] and VEON [73], which are specifically designed for open-vocabulary occupancy estimation in surrounding-view scenes. In addition, OccGS improves the performance of our baseline method GaussianOcc [12] by 19.00 in terms of mIoU. While the aforementioned approaches do not require additional supervision, they struggle with efficiently

modeling semantic geometry and neglect dynamic objects, leading to performance degradation.

Qualitative results. As shown in Figure 4, the occupancy estimated by OccGS excels in scene completeness, consistency, and dynamic object handling, achieving results comparable to manually labeled GT. Furthermore, OccGS performs robustly in extreme weather conditions (*e.g.*, rain, fog, *etc.*). As illustrated in Figure 4, in areas where ground truth is missing due to rain, OccGS successfully reconstructs both the geometry and semantics of the road surface.

4.4. Zero-shot Occupancy Estimation

SemanticKITTI differs from Occ3D-nuScenes in terms of semantic categories, sensor parameters, and voxel size. To evaluate the zero-shot generalization ability, we compare our approach with methods employing different training strategies on Occ3D-nuScenes (including supervision by 3D and 2D GT and self-supervision), directly performing inference on SemanticKITTI without retraining.

Across the base semantic categories (as seen in the training set), Table 2 shows that all other methods [12, 18, 46, 59, 66] suffer significant performance degradation, as they are tailored to specific camera parameters and occupancy distributions. For novel classes unseen during training, these methods fail to perform open-vocabulary occupancy estimation. In contrast, OccGS enables zero-shot learning for unseen scenes and supports open-vocabulary semantic occupancy estimation, demonstrating strong generalization and flexibility. We also evaluate our approach against OVO [46], which is specifically designed for open-vocabulary occupancy estimation in monocular scenes. Table 2 shows OccGS performs favorably against OVO

Table 3. **Comparisons of representation characteristics and model efficiency.** Label-free means training without any human-labeled annotations. Open-vocabulary stands for the prediction capability for unseen classes. Zero-shot highlights models capable of zero-shot learning for unseen scenes, demonstrating strong cross-dataset generalization. † indicates the use of pre-trained models to obtain 2D semantic segmentation results before training.

Method	Representation	Latency (ms)	Memory (G)	Label-free	Open-vocabulary	Zero-shot
MonoScene [4]	3D Voxel	608	20.3	✗	✗	✗
BEVFormer [27]	2D BEV	302	24.5	✗	✗	✗
TPVFormer [59]	2.5D TPV	341	28.3	✗	✗	✗
FB-Occ [28]	2D BEV+3D Voxel	463	30.3	✗	✗	✗
GaussianFormer [18]	Gaussian	312	6.1	✗	✗	✗
SurroundOcc [56]	3D Voxel	295	35	✗	✗	✗
SimpleOcc [14]	NeRF	172	56.1	✗	✗	✗
RenderOcc [37]	NeRF	116	22.4	✗	✗	✗
OccNeRF [66] †	NeRF	93	77.1	✓	✗	✗
GaussianOcc [12] †	Gaussian	95	32.7	✓	✗	✗
POP-3D [52] †	Voxel	524	39.5	✓	✓	✗
OVO [46] †	Voxel	647	42.4	✓	✓	✗
Ours †	Improved Gaussian	82	4.8	✓	✓	✓

in single-front-view scenarios (*e.g.*, SemanticKITTI). The qualitative comparisons of zero-shot cross dataset validation on SemanticKITTI [1] are shown in Figure 3.

4.5. Representation Efficiency Analysis

Table 3 presents evaluations on representation characteristics and model efficiency. Notably, OccGS excels in inference latency, being three times faster than TPVFormer [59] and outpacing other NeRF-based [14, 37, 66] and Gaussian-based approaches [12, 18]. Leveraging the proposed efficient representation SGAG, our method demonstrates an advantage in computational cost, delivering better performance with reduced memory requirements. In contrast, scene representations based on dense voxels [4, 28] and BEV [27] incur redundant computational costs, while NeRF-based methods [37, 66] rely on dense sampling, leading to heavy computational loads. In addition, OccGS strikes a balance between efficiency and flexibility, enabling zero-shot scene-aware occupancy reconstruction, supporting open-vocabulary semantic occupancy estimation, and requiring no human-labeled annotations.

4.6. Ablation Studies

We analyze the effect of dynamic objects clustering (DOC) by disabling the clustering of dynamic objects and optimizing them together with static foregrounds. Table 4 and Figure 5 show that dynamic objects clustering effectively mitigates the challenges of dynamic trailing and spatial occlusion in occupancy estimation. Table 4 foreground-background decoupling also facilitates fine-grained, object-level estimation of semantic occupancy. We further ablate the effect of LiDAR geometric priors by removing the L_{geo} loss from our framework. The degraded results highlight the importance of geometric priors in constraining the shape and distribution of Gaussians, thereby enabling a more ac-

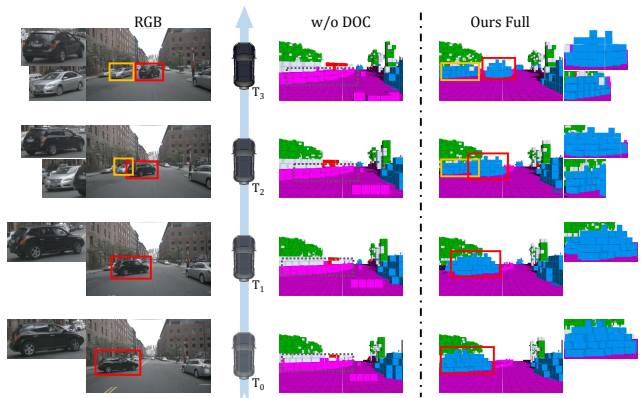


Figure 5. **Semantic 3D Occupancy of dynamic objects.** OccGS accurately estimates the semantic occupancy of dynamic objects, maintains spatiotemporal consistency, and infers occluded parts.

Table 4. **Effect of each module in our method.** DOC and FBD are short for the dynamic objects clustering and foreground background decoupling, respectively.

Model	IoU ↑	mIoU ↑
w/o DOC	82.65	26.84
w/o FBD	81.03	28.41
w/o L_{geo}	83.49	29.36
OccGS-Z	<u>83.82</u>	30.26
OccGS-S	83.10	<u>36.99</u>

curate reconstruction of the overall scene structure. More quantitative and qualitative results are available in the supplementary material.

5. Conclusion

In this paper, we present a novel framework (OccGS) that enables zero-shot open-vocabulary semantic occupancy reconstruction without the need for any manually-labeled annotations. To facilitate scene understanding, we leverage VLMs and multimodal geometric priors to construct a Se-

semantic and Geometric-Aware Gaussian representation. Together with cumulative Gaussian-to-3D voxel splatting, OcGS strikes a balance between accuracy and efficiency. Our framework achieves state-of-the-art performance on zero-shot semantic occupancy estimation and performs favorably against supervised and self-supervised approaches.

References

- [1] Jens Behley, Martin Garbade, Andres Milioto, Jan Quenzel, Sven Behnke, Cyrill Stachniss, and Jurgen Gall. Semantickitti: A dataset for semantic scene understanding of lidar sequences. In *ICCV*, pages 9297–9307, 2019. [6](#), [8](#), [12](#), [14](#), [15](#), [16](#)
- [2] Simon Boeder, Fabian Gigengack, and Benjamin Risse. Langocc: Self-supervised open vocabulary occupancy estimation via volume rendering. *arXiv preprint arXiv:2407.17310*, 2024. [2](#), [5](#), [6](#), [7](#), [13](#), [15](#)
- [3] Simon Boeder, Fabian Gigengack, and Benjamin Risse. Ocflownet: Towards self-supervised occupancy estimation via differentiable rendering and occupancy flow. *arXiv preprint arXiv:2402.12792*, 2024. [1](#), [2](#)
- [4] Anh-Quan Cao and Raoul De Charette. Monoscene: Monocular 3d semantic scene completion. In *CVPR*, pages 3991–4001, 2022. [2](#), [5](#), [6](#), [8](#), [13](#), [15](#)
- [5] Loick Chambon, Eloi Zablocki, Mickaël Chen, Florent Bar-toccioni, Patrick Pérez, and Matthieu Cord. Pointbev: A sparse approach for bev predictions. In *CVPR*, pages 15195–15204, 2024. [2](#)
- [6] Devendra Singh Chaplot, Murtaza Dalal, Saurabh Gupta, Jitendra Malik, and Russ R Salakhutdinov. Seal: Self-supervised embodied active learning using exploration and 3d consistency. *NIPS*, 34:13086–13098, 2021. [1](#)
- [7] Yukang Chen, Jianhui Liu, Xiangyu Zhang, Xiaojuan Qi, and Jiaya Jia. Voxelnex: Fully sparse voxelnet for 3d object detection and tracking. In *CVPR*, pages 21674–21683, 2023. [2](#), [13](#), [15](#)
- [8] Jiadi Cui, Junming Cao, Yuhui Zhong, Liao Wang, Fuqiang Zhao, Penghao Wang, Yifan Chen, Zhipeng He, Lan Xu, Yujiao Shi, et al. Letsgo: Large-scale garage modeling and rendering via lidar-assisted gaussian primitives. *arXiv preprint arXiv:2404.09748*, 2024. [13](#)
- [9] Pierre Dellenbach, Jean-Emmanuel Deschaud, Bastien Jacquet, and François Goulette. Ct-icp: Real-time elastic lidar odometry with loop closure. In *ICRA*, pages 5580–5586. IEEE, 2022. [4](#)
- [10] Ayush Dewan, Tim Caselitz, Gian Diego Tipaldi, and Wolfram Burgard. Rigid scene flow for 3d lidar scans. In *IROS*, pages 1765–1770. IEEE, 2016. [4](#)
- [11] Tobias Fischer, Jonas Kulhanek, Samuel Rota Buló, Lorenzo Porzi, Marc Pollefeys, and Peter Kotschieder. Dynamic 3d gaussian fields for urban areas. *arXiv preprint arXiv:2406.03175*, 2024. [3](#)
- [12] Wanshui Gan, Fang Liu, Hongbin Xu, Ningkai Mo, and Naoto Yokoya. Gaussianocc: Fully self-supervised and efficient 3d occupancy estimation with gaussian splatting. *arXiv preprint arXiv:2408.11447*, 2024. [1](#), [2](#), [3](#), [4](#), [5](#), [6](#), [7](#), [8](#), [13](#), [14](#), [15](#), [16](#)
- [13] Wanshui Gan, Ningkai Mo, Hongbin Xu, and Naoto Yokoya. A comprehensive framework for 3d occupancy estimation in autonomous driving. *IEEE Transactions on Intelligent Vehicles*, 2024. [1](#), [2](#), [5](#), [13](#)
- [14] Adam W Harley, Zhaoyuan Fang, Jie Li, Rares Ambrus, and Katerina Fragkiadaki. Simple-bev: What really matters for multi-sensor bev perception? In *ICRA*, pages 2759–2765. IEEE, 2023. [2](#), [6](#), [7](#), [8](#), [14](#), [15](#)
- [15] Xu Hu, Yuxi Wang, Lue Fan, Junsong Fan, Junran Peng, Zhen Lei, Qing Li, and Zhaoxiang Zhang. Semantic anything in 3d gaussians. *arXiv preprint arXiv:2401.17857*, 2024. [3](#)
- [16] Yuanhui Huang, Wenzhao Zheng, Yunpeng Zhang, Jie Zhou, and Jiwen Lu. Tri-perspective view for vision-based 3d semantic occupancy prediction. In *CVPR*, pages 9223–9232, 2023. [1](#), [2](#)
- [17] Yuanhui Huang, Wenzhao Zheng, Borui Zhang, Jie Zhou, and Jiwen Lu. Selfocc: Self-supervised vision-based 3d occupancy prediction. In *CVPR*, pages 19946–19956, 2024. [1](#), [2](#), [5](#), [6](#), [13](#), [14](#), [15](#)
- [18] Yuanhui Huang, Wenzhao Zheng, Yunpeng Zhang, Jie Zhou, and Jiwen Lu. Gaussianformer: Scene as gaussians for vision-based 3d semantic occupancy prediction. *arXiv preprint arXiv:2405.17429*, 2024. [3](#), [5](#), [6](#), [7](#), [8](#), [13](#), [15](#), [16](#)
- [19] Lei Ke, Mingqiao Ye, Martin Danelljan, Yu-Wing Tai, Chi-Keung Tang, Fisher Yu, et al. Segment anything in high quality. *NIPS*, 36, 2024. [3](#), [12](#)
- [20] Bernhard Kerbl, Georgios Kopanas, Thomas Leimkühler, and George Drettakis. 3d gaussian splatting for real-time radiance field rendering. *ACM Trans. Graph.*, 42(4):139–1, 2023. [3](#), [13](#)
- [21] Alexander Kirillov, Eric Mintun, Nikhila Ravi, Hanzi Mao, Chloe Rolland, Laura Gustafson, Tete Xiao, Spencer Whitehead, Alexander C Berg, Wan-Yen Lo, et al. Segment anything. In *ICCV*, pages 4015–4026, 2023. [3](#), [12](#)
- [22] Weicheng Kuo, Yin Cui, Xiuye Gu, AJ Piergiovanni, and Anelia Angelova. F-vm: Open-vocabulary object detection upon frozen vision and language models. *arXiv preprint arXiv:2209.15639*, 2022. [3](#)
- [23] Yanwei Li, Yilun Chen, Xiaojuan Qi, Zeming Li, Jian Sun, and Jiaya Jia. Unifying voxel-based representation with transformer for 3d object detection. *NIPS*, 35:18442–18455, 2022. [2](#)
- [24] Yanwei Li, Xiaojuan Qi, Yukang Chen, Liwei Wang, Zeming Li, Jian Sun, and Jiaya Jia. Voxel field fusion for 3d object detection. In *CVPR*, pages 1120–1129, 2022. [2](#)
- [25] Yin hao Li, Han Bao, Zheng Ge, Jinrong Yang, Jianjian Sun, and Zeming Li. Bevstereo: Enhancing depth estimation in multi-view 3d object detection with temporal stereo. In *AAAI*, pages 1486–1494, 2023. [5](#), [6](#), [13](#), [15](#)
- [26] Yangguang Li, Bin Huang, Zeren Chen, Yufeng Cui, Feng Liang, Mingzhu Shen, Fenggang Liu, Enze Xie, Lu Sheng, Wanli Ouyang, et al. Fast-bev: A fast and strong bird’s-eye view perception baseline. *TPAMI*, 2024. [2](#)
- [27] Zhiqi Li, Wenhai Wang, Hongyang Li, Enze Xie, Chonghao Sima, Tong Lu, Yu Qiao, and Jifeng Dai. Bevformer: Learning bird’s-eye-view representation from multi-camera images via spatiotemporal transformers. In *ECCV*, pages 1–18. Springer, 2022. [1](#), [2](#), [5](#), [6](#), [8](#), [13](#), [15](#)

- [28] Zhiqi Li, Zhiding Yu, David Austin, Mingsheng Fang, Shiyi Lan, Jan Kautz, and Jose M Alvarez. Fb-occ: 3d occupancy prediction based on forward-backward view transformation. *arXiv preprint arXiv:2307.01492*, 2023. 1, 2, 5, 6, 8, 13, 15
- [29] Yancong Lin and Holger Caesar. Icp-flow: Lidar scene flow estimation with icp. In *CVPR*, pages 15501–15511, 2024. 4
- [30] Shilong Liu, Zhaoyang Zeng, Tianhe Ren, Feng Li, Hao Zhang, Jie Yang, Qing Jiang, Chunyuan Li, Jianwei Yang, Hang Su, et al. Grounding dino: Marrying dino with grounded pre-training for open-set object detection. *arXiv preprint arXiv:2303.05499*, 2023. 3, 4, 12
- [31] Tianqi Liu, Guangcong Wang, Shoukang Hu, Liao Shen, Xinyi Ye, Yuhang Zang, Zhiguo Cao, Wei Li, and Ziwei Liu. Mvsgaussian: Fast generalizable gaussian splatting reconstruction from multi-view stereo. In *ECCV*, pages 37–53. Springer, 2025. 4
- [32] Zhijian Liu, Haotian Tang, Alexander Amini, Xinyu Yang, Huizi Mao, Daniela L Rus, and Song Han. Bevfusion: Multi-task multi-sensor fusion with unified bird’s-eye view representation. In *ICRA*, pages 2774–2781. IEEE, 2023. 13, 15
- [33] Yunze Man, Liang-Yan Gui, and Yu-Xiong Wang. Bev-guided multi-modality fusion for driving perception. In *CVPR*, pages 21960–21969, 2023. 2
- [34] Ben Mildenhall, Pratul P Srinivasan, Matthew Tancik, Jonathan T Barron, Ravi Ramamoorthi, and Ren Ng. Nerf: Representing scenes as neural radiance fields for view synthesis. *Communications of the ACM*, 65(1):99–106, 2021. 2
- [35] Jingyi Pan, Zipeng Wang, and Lin Wang. Co-occ: Coupling explicit feature fusion with volume rendering regularization for multi-modal 3d semantic occupancy prediction. *IEEE Robotics and Automation Letters*, 2024. 13, 15
- [36] Mingjie Pan, Li Liu, Jiaming Liu, Peixiang Huang, Longlong Wang, Shanghang Zhang, Shaoqing Xu, Zhiyi Lai, and Kuiyuan Yang. Uniocc: Unifying vision-centric 3d occupancy prediction with geometric and semantic rendering. *arXiv preprint arXiv:2306.09117*, 2023. 1, 2
- [37] Mingjie Pan, Jiaming Liu, Renrui Zhang, Peixiang Huang, Xiaoqi Li, Hongwei Xie, Bing Wang, Li Liu, and Shanghang Zhang. Renderocc: Vision-centric 3d occupancy prediction with 2d rendering supervision. In *ICRA*, pages 12404–12411. IEEE, 2024. 2, 5, 6, 7, 8, 13, 14, 15
- [38] Minghan Qin, Wanhua Li, Jiawei Zhou, Haoqian Wang, and Hanspeter Pfister. Langsplat: 3d language gaussian splatting. In *CVPR*, pages 20051–20060, 2024. 3
- [39] Santhosh K Ramakrishnan, Ziad Al-Halah, and Kristen Grauman. Occupancy anticipation for efficient exploration and navigation. In *ECCV*, pages 400–418. Springer, 2020. 1
- [40] Santhosh K Ramakrishnan, Dinesh Jayaraman, and Kristen Grauman. An exploration of embodied visual exploration. *IJCV*, 129(5):1616–1649, 2021. 1
- [41] Nikhila Ravi, Valentin Gabeur, Yuan-Ting Hu, Ronghang Hu, Chaitanya Ryali, Tengyu Ma, Haitham Khedr, Roman Rädle, Chloe Rolland, Laura Gustafson, et al. Sam 2: Segment anything in images and videos. *arXiv preprint arXiv:2408.00714*, 2024. 4
- [42] Tianhe Ren, Shilong Liu, Ailing Zeng, Jing Lin, Kunchang Li, He Cao, Jiayu Chen, Xinyu Huang, Yukang Chen, Feng Yan, et al. Grounded sam: Assembling open-world models for diverse visual tasks. *arXiv preprint arXiv:2401.14159*, 2024. 3, 12
- [43] Johannes L Schonberger and Jan-Michael Frahm. Structure-from-motion revisited. In *CVPR*, pages 4104–4113, 2016. 16
- [44] Yiang Shi, Tianheng Cheng, Qian Zhang, Wenyu Liu, and Xinggang Wang. Occupancy as set of points. *arXiv preprint arXiv:2407.04049*, 2024. 2
- [45] Noah Snavely, Steven M Seitz, and Richard Szeliski. Photo tourism: exploring photo collections in 3d. In *ACM SIGGRAPH*, pages 835–846, 2006. 16
- [46] Zhiyu Tan, Zichao Dong, Cheng Zhang, Weikun Zhang, Hang Ji, and Hao Li. Ovo: Open-vocabulary occupancy. *arXiv preprint arXiv:2305.16133*, 2023. 6, 7, 8
- [47] Matthew Tancik, Vincent Casser, Xinchen Yan, Sabeek Pradhan, Ben Mildenhall, Pratul P Srinivasan, Jonathan T Barron, and Henrik Kretzschmar. Block-nerf: Scalable large scene neural view synthesis. In *CVPR*, pages 8248–8258, 2022. 2
- [48] Ayush Tewari, Ohad Fried, Justus Thies, Vincent Sitzmann, Stephen Lombardi, Kalyan Sunkavalli, Ricardo Martin-Brualla, Tomas Simon, Jason Saragih, Matthias Nießner, et al. State of the art on neural rendering. In *Computer Graphics Forum*, pages 701–727. Wiley Online Library, 2020. 2
- [49] Qijian Tian, Xin Tan, Yuan Xie, and Lizhuang Ma. Drivingforward: Feed-forward 3d gaussian splatting for driving scene reconstruction from flexible surround-view input. *arXiv preprint arXiv:2409.12753*, 2024. 3
- [50] Xiaoyu Tian, Tao Jiang, Longfei Yun, Yucheng Mao, Huitong Yang, Yue Wang, Yilun Wang, and Hang Zhao. Occ3d: A large-scale 3d occupancy prediction benchmark for autonomous driving. *NIPS*, 36, 2024. 2, 5, 6, 7, 12, 13, 14, 15, 16
- [51] Wenwen Tong, Chonghao Sima, Tai Wang, Li Chen, Silei Wu, Hanming Deng, Yi Gu, Lewei Lu, Ping Luo, Dahua Lin, et al. Scene as occupancy. In *ICCV*, pages 8406–8415, 2023. 1
- [52] Antonin Vobecky, Oriane Siméoni, David Hurych, Spyridon Gidaris, Andrei Bursuc, Patrick Pérez, and Josef Sivic. Pop-3d: Open-vocabulary 3d occupancy prediction from images. *NIPS*, 36, 2024. 2, 8
- [53] Lizi Wang, Hongkai Ye, Qianhao Wang, Yuman Gao, Chao Xu, and Fei Gao. Learning-based 3d occupancy prediction for autonomous navigation in occluded environments. In *IROS*, pages 4509–4516. IEEE, 2021. 1
- [54] Xiaofeng Wang, Zheng Zhu, Wenbo Xu, Yunpeng Zhang, Yi Wei, Xu Chi, Yun Ye, Dalong Du, Jiwen Lu, and Xinggang Wang. Openoccupancy: A large scale benchmark for surrounding semantic occupancy perception. In *ICCV*, pages 17850–17859, 2023. 2
- [55] Yuqi Wang, Yuntao Chen, Xingyu Liao, Lue Fan, and Zhaoxiang Zhang. Panoocc: Unified occupancy representation for camera-based 3d panoptic segmentation. In *CVPR*, pages 17158–17168, 2024. 1
- [56] Yi Wei, Linqing Zhao, Wenzhao Zheng, Zheng Zhu, Jie Zhou, and Jiwen Lu. Surroundocc: Multi-camera 3d occu-

- pancy prediction for autonomous driving. In *ICCV*, pages 21729–21740, 2023. [5](#), [6](#), [8](#), [13](#), [15](#)
- [57] Minye Wu, Zehao Wang, Georgios Kouros, and Tinne Tuytelaars. Tetrif: Temporal tri-plane radiance fields for efficient free-viewpoint video. In *CVPR*, pages 6487–6496, 2024. [2](#)
- [58] Hu Xu, Gargi Ghosh, Po-Yao Huang, Prahal Arora, Masoumeh Aminzadeh, Christoph Feichtenhofer, Florian Metze, and Luke Zettlemoyer. Vlm: Task-agnostic video-language model pre-training for video understanding. *arXiv preprint arXiv:2105.09996*, 2021. [3](#)
- [59] Zhiqiang Yan, Yuankai Lin, Kun Wang, Yupeng Zheng, Yufei Wang, Zhenyu Zhang, Jun Li, and Jian Yang. Tri-perspective view decomposition for geometry-aware depth completion. In *CVPR*, pages 4874–4884, 2024. [2](#), [5](#), [6](#), [7](#), [8](#), [13](#), [15](#), [16](#)
- [60] Chenyu Yang, Yuntao Chen, Hao Tian, Chenxin Tao, Xizhou Zhu, Zhaoxiang Zhang, Gao Huang, Hongyang Li, Yu Qiao, Lewei Lu, et al. Bevformer v2: Adapting modern image backbones to bird’s-eye-view recognition via perspective supervision. In *CVPR*, pages 17830–17839, 2023. [1](#)
- [61] Zhengyuan Yang, Songyang Zhang, Liwei Wang, and Jiebo Luo. Sat: 2d semantics assisted training for 3d visual grounding. In *ICCV*, pages 1856–1866, 2021. [3](#)
- [62] Chongjie Ye, Yinyu Nie, Jiahao Chang, Yuntao Chen, Yihao Zhi, and Xiaoguang Han. Gaustudio: A modular framework for 3d gaussian splatting and beyond. *arXiv preprint arXiv:2403.19632*, 2024. [12](#)
- [63] Heng Yu, Joel Julin, Zoltán Á Milacski, Koichiro Niinuma, and László A Jeni. Cogs: Controllable gaussian splatting. In *CVPR*, pages 21624–21633, 2024. [13](#)
- [64] Zichen Yu, Changyong Shu, Jiajun Deng, Kangjie Lu, Zongdai Liu, Jiangyong Yu, Dawei Yang, Hui Li, and Yan Chen. Flashocc: Fast and memory-efficient occupancy prediction via channel-to-height plugin. *arXiv preprint arXiv:2311.12058*, 2023. [1](#), [2](#)
- [65] Zehao Yu, Anpei Chen, Binbin Huang, Torsten Sattler, and Andreas Geiger. Mip-splatting: Alias-free 3d gaussian splatting. In *CVPR*, pages 19447–19456, 2024. [3](#)
- [66] Chubin Zhang, Juncheng Yan, Yi Wei, Jiabin Li, Li Liu, Yansong Tang, Yueqi Duan, and Jiwen Lu. Occnerf: Self-supervised multi-camera occupancy prediction with neural radiance fields. *arXiv e-prints*, pages arXiv–2312, 2023. [1](#), [2](#), [5](#), [6](#), [7](#), [8](#), [13](#), [14](#), [15](#), [16](#)
- [67] Dingyuan Zhang, Dingkan Liang, Hongcheng Yang, Zhikang Zou, Xiaoqing Ye, Zhe Liu, and Xiang Bai. Sam3d: Zero-shot 3d object detection via segment anything model. *arXiv preprint arXiv:2306.02245*, 2023. [3](#)
- [68] Yunpeng Zhang, Zheng Zhu, and Dalong Du. Occformer: Dual-path transformer for vision-based 3d semantic occupancy prediction. In *ICCV*, pages 9433–9443, 2023. [2](#), [5](#), [6](#), [13](#), [15](#)
- [69] Zheng Zhang, Wenbo Hu, Yixing Lao, Tong He, and Hengshuang Zhao. Pixel-gs: Density control with pixel-aware gradient for 3d gaussian splatting. *arXiv preprint arXiv:2403.15530*, 2024. [13](#)
- [70] Cheng Zhao, Su Sun, Ruoyu Wang, Yuliang Guo, Jun-Jun Wan, Zhou Huang, Xinyu Huang, Yingjie Victor Chen, and Liu Ren. Telc-gs: Tightly coupled lidar-camera gaussian splatting for surrounding autonomous driving scenes. *arXiv preprint arXiv:2404.02410*, 2024. [12](#), [13](#)
- [71] Lin Zhao, Hui Zhou, Xinge Zhu, Xiao Song, Hongsheng Li, and Wenbing Tao. Lif-seg: Lidar and camera image fusion for 3d lidar semantic segmentation. *IEEE Transactions on Multimedia*, 26:1158–1168, 2023. [4](#)
- [72] Xiangmo Zhao, Pengpeng Sun, Zhigang Xu, Haigen Min, and Hongkai Yu. Fusion of 3d lidar and camera data for object detection in autonomous vehicle applications. *IEEE Sensors Journal*, 20(9):4901–4913, 2020. [4](#)
- [73] Jilai Zheng, Pin Tang, Zhongdao Wang, Guoqing Wang, Xianguan Ren, Bailan Feng, and Chao Ma. Veon: Vocabulary-enhanced occupancy prediction. In *ECCV*, pages 92–108. Springer, 2025. [5](#), [6](#), [7](#), [13](#), [15](#)
- [74] Hongyu Zhou, Jiahao Shao, Lu Xu, Dongfeng Bai, Weichao Qiu, Bingbing Liu, Yue Wang, Andreas Geiger, and Yiyi Liao. Hugs: Holistic urban 3d scene understanding via gaussian splatting. In *CVPR*, pages 21336–21345, 2024. [12](#)
- [75] Xiaoyu Zhou, Zhiwei Lin, Xiaojun Shan, Yongtao Wang, Deqing Sun, and Ming-Hsuan Yang. Drivinggaussian: Composite gaussian splatting for surrounding dynamic autonomous driving scenes. In *CVPR*, pages 21634–21643, 2024. [3](#), [12](#)

OccGS: Zero-shot 3D Occupancy Reconstruction with Semantic and Geometric-Aware Gaussian Splatting

Supplementary Material

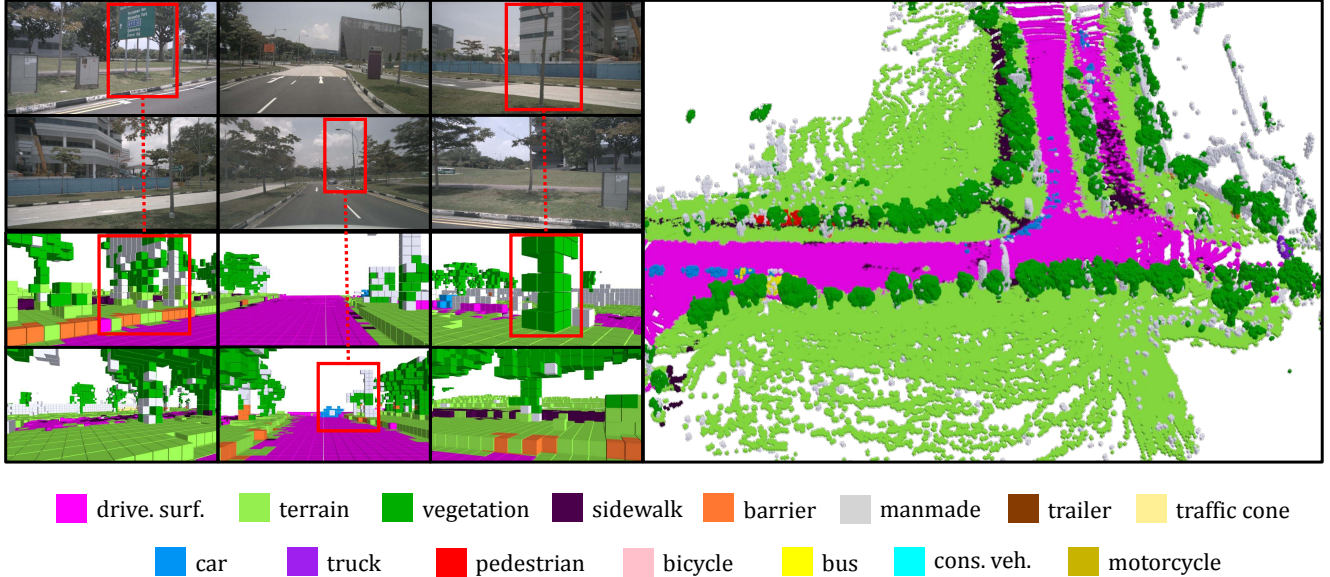


Figure 6. **Qualitative results of OccGS for semantic 3D occupancy reconstruction.** The results highlight the promising performance of our method, achieving high-quality and comprehensive semantic occupancy, even in challenging cases involving irregular geometric structures and intricate objects at distant ranges.

We present further implementation details, quantitative and qualitative experimental results, ablation studies, and failure cases in the supplementary material:

- Section A: Additional implementation details.
- Section B: Additional quantitative and qualitative results.
- Section C: Additional ablation studies.
- Section D: Failure cases and limitations.

A. Additional Implementation Details

Details of VLMs-guided Semantics. We integrate Grounding-DINO [30, 42] with SAM [19, 21] to obtain open-vocabulary 2D semantic priors. For open-set object detection, we first employ Grounding-DINO to extract 2D bounding boxes for objects belonging to the target semantic categories. SAM is then utilized to generate pixel-level segmentation masks within the areas defined by the bounding boxes. Notably, neither of the VLM models is exposed to nuScenes [50] or KITTI [1] data during training, ensuring that the validation sets remain entirely unseen by these methods, thereby guaranteeing the effectiveness of zero-shot evaluation. We conduct extended experiments in Section C to compare the semantics extracted by VLMs with 2D ground truth derived from 3D manual annotations.

To ensure instance-level semantic consistency for dy-

namic objects, we align LiDAR points with 2D segmentations in 3D space. Specifically, we project LiDAR points onto the 2D segmentations to assign corresponding semantics. These points are then back-projected into 3D space, where clusters of nearby points sharing the same semantics are identified as belonging to the same instance. The clusters are further refined across multiple frames of LiDAR and image data to minimize the impact of occluded regions.

Details of Sky Areas. Gaussians often generate cloud-like artifacts in the foreground when modeling the sky, which degrades the quality of semantic occupancy reconstruction. To address this, our framework leverages both semantic and geometric priors to distinguish sky regions from the foreground. Similar to [62, 74], we utilize semantic masks of the sky generated by VLMs and penalize the opacity values α_{sky} within the sky region to approach zero. Additionally, we incorporate the LiDAR prior and geometric loss L_{geo} to constrain the Gaussians away from the sky, effectively reducing floaters from these infinitely distant regions.

Details of LiDAR-guided Geometry. Despite the sparsity of LiDAR points collected by sensors, they still provide valuable geometric priors for 3DGS, as highlighted by [70, 75]. In the Semantic and Geometric-Aware Gaussians (SGAG), we initialize the Gaussians using the semantic LiDAR points obtained in Section A and constrain the

Table 5. **3D occupancy estimation on Occ3D-nuScenes [50]**. 3D Occ refers to annotated occupancy GT, LiDAR denotes manually labeled semantic point clouds, 2D represents 2D semantic labels derived from 3D, and N/A indicates the absence of manual annotations. “cons. veh.” and “drive. surf.” stand for construction vehicles and driveable surfaces, respectively. TPVFormer* is trained with labeled LiDAR. VoxelNet* is trained with labeled 3D GT, using LiDAR as input. Co-Occ [35] and BEVFusion [32] utilize multimodal inputs, including multi-view images and LiDAR. OccGS-Z is the version of OccGS without using any manual labels, while OccGS-S adopts 2D semantic annotations from [37]. The intersection over union (IoU) and mean IoU of semantic classes (mIoU) are calculated over all voxels.

Method	Supervision	IoU ↑	mIoU ↑	Semantic Classes															
				barrier	bicycle	bus	car	cons. veh.	motorcycle	pedestrian	traffic cone	trailer	truck	drive. surf.	sidewalk	terrain	manmade	vegetation	
MonoScene [4]	3D Occ	-	6.33	7.23	4.26	4.93	9.38	5.67	3.98	3.01	5.90	4.45	7.17	14.91	7.92	7.43	1.01	7.65	
BEVStereo [25]	3D Occ	-	25.47	38.41	7.88	38.7	41.2	17.56	17.33	14.69	10.31	16.84	29.62	54.08	32.68	26.54	18.74	17.49	
BEVFormer [27]	3D Occ	-	28.19	37.83	17.87	40.44	42.43	7.36	23.88	21.81	20.98	22.38	30.70	55.35	36.00	28.06	20.04	17.69	
OccFormer [68]	3D Occ	30.13	22.40	30.29	12.32	34.40	39.17	14.44	16.45	17.22	9.27	13.90	26.36	50.99	34.66	22.73	6.76	6.97	
TPVFormer [59]	3D Occ	66.80	28.70	38.90	13.67	40.78	45.90	17.23	19.99	18.85	14.30	26.69	34.17	55.65	37.55	30.70	19.40	16.78	
TPVFormer* [59]	LiDAR	17.20	13.89	14.82	9.43	21.30	16.79	14.51	13.82	11.24	5.35	16.17	19.70	10.81	9.52	11.24	16.57	17.03	
FB-Occ [28]	3D Occ	<u>77.45</u>	28.87	40.91	21.22	39.17	40.80	20.61	23.78	23.62	25.03	16.61	26.35	59.42	31.43	29.02	16.67	18.42	
CTF-Occ [50]	3D Occ	-	29.54	39.33	20.56	38.29	42.24	16.93	24.52	22.72	21.05	22.98	31.11	53.33	37.98	33.23	20.79	18.00	
Co-Occ [35]	3D Occ	-	27.17	28.10	16.10	34.00	37.20	17.00	21.60	20.80	15.90	21.90	28.70	42.30	29.10	28.60	28.20	38.00	
BEVFusion [32]	3D Occ	-	<u>33.45</u>	42.69	22.00	38.88	43.79	23.86	27.58	22.24	22.83	28.38	35.79	45.50	31.08	29.31	45.04	43.62	
VoxelNet* [7]	3D Occ	-	26.39	36.96	11.15	25.60	26.42	18.97	15.02	9.69	7.82	22.48	23.69	46.59	30.97	28.85	45.73	45.97	
GaussianFormer [18]	3D Occ	-	18.82	19.52	11.26	26.11	29.78	10.47	13.83	12.58	8.67	12.74	21.57	39.63	24.46	22.99	9.59	19.12	
SurroundOcc [56]	3D Occ	-	20.07	20.59	11.68	28.06	30.86	10.70	15.14	14.09	12.06	14.38	22.26	37.29	24.49	22.77	14.89	21.86	
RenderOcc [37]	2D	-	24.52	27.56	14.36	19.91	20.56	11.96	12.42	12.14	14.34	20.81	18.94	68.85	42.01	43.94	17.36	22.61	
SimpleOcc [13]	2D	42.78	7.99	0.67	1.18	3.21	7.63	1.02	0.26	1.80	0.26	1.07	2.81	40.44	18.30	17.01	13.42	10.84	
OccGS-S	2D	<u>83.10</u>	<u>36.99</u>	<u>31.67</u>	<u>19.18</u>	<u>20.42</u>	<u>32.25</u>	<u>24.28</u>	<u>14.20</u>	<u>23.98</u>	<u>39.53</u>	<u>18.05</u>	<u>29.91</u>	<u>62.05</u>	<u>40.48</u>	<u>43.32</u>	<u>72.33</u>	<u>83.26</u>	
SelfOcc [17]	N/A	45.01	10.57	0.21	0.73	5.50	12.52	0.10	0.82	2.09	0.00	0.00	8.31	55.53	26.30	26.62	14.21	5.64	
OccNeRF [66]	N/A	53.57	10.81	0.83	0.82	5.13	12.49	3.50	0.23	3.10	1.84	0.52	3.90	52.62	20.81	24.75	18.45	13.19	
GaussianOcc [12]	N/A	-	11.26	1.79	5.82	14.58	13.55	1.30	2.82	7.95	9.76	0.56	9.61	44.59	20.10	17.58	8.61	10.29	
LangOcc [2]	N/A	51.60	12.05	2.73	7.21	5.78	13.92	0.51	10.80	6.42	8.67	3.24	11.02	42.10	12.44	27.17	14.13	14.55	
VEON [73]	N/A	-	13.98	4.80	2.70	14.70	10.90	11.00	3.80	4.70	4.00	5.30	9.60	46.50	21.10	22.10	24.80	23.70	
OccGS-Z	N/A	<u>83.82</u>	<u>30.26</u>	13.50	20.10	18.63	33.79	12.18	17.54	30.18	28.58	2.18	23.75	62.67	29.89	36.81	55.24	68.83	

geometric distribution of the Gaussian ellipsoids through the geometric loss term L_{geo} . We validate the effectiveness of LiDAR-guided geometry in Section C by comparing it with various point cloud initialization methods.

Due to the sparsity and limited range of LiDAR points, they cannot fully cover the entire scene. To address this limitation, we adopt the adaptive control of Gaussians introduced by [20, 63, 69], which targets regions with missing geometric features. By applying semantic-specific thresholds, we adaptively densify Gaussians, enabling them to “grow” according to their semantic context and achieve a more accurate representation of the occupancy geometry. This strategy has proven effective in addressing missing geometric regions, particularly under challenging conditions for LiDAR, such as rain-soaked road surfaces.

Details of Cumulative Gaussian-to-3D voxel Splatting.

We propose cumulative Gaussian-to-3D voxel splatting to reconstruct semantic occupancy from SGAG. As illustrated in Figure 7, the Gaussians in SGAG do not have an explicit correspondence with voxels. Instead, voxel features are derived through a process of cumulative probability accumulation from the Gaussians. Inspired by [8, 70], we avoid directly assigning semantic weights based on the distance between the Gaussian center and the voxel, as Gaussians

vary in size, shape, and orientation. Instead, by accumulating the weights of Gaussian value $G(x)$, occupied range d , and opacity α passing through each voxel, we effectively reconstruct dense occupancy from the sparse Gaussian distribution while preserving the accuracy of semantic results.

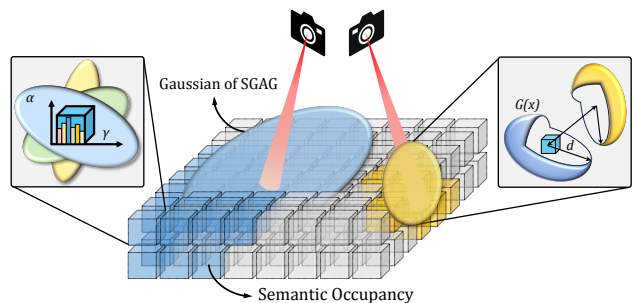


Figure 7. **Cumulative Gaussian-to-3D voxel splatting.** We propose an implicit cumulative splatting strategy that ensures both efficient and high-quality conversion from Gaussians to voxels.

Details of Experimental Setup. For 3D occupancy reconstruction on the Occ3D-nuScenes [50] dataset, we use the predefined range of [-40m, -40m, -1m, 40m, 40m, 5.4m] with a voxel size of 0.4m. We train using only keyframes

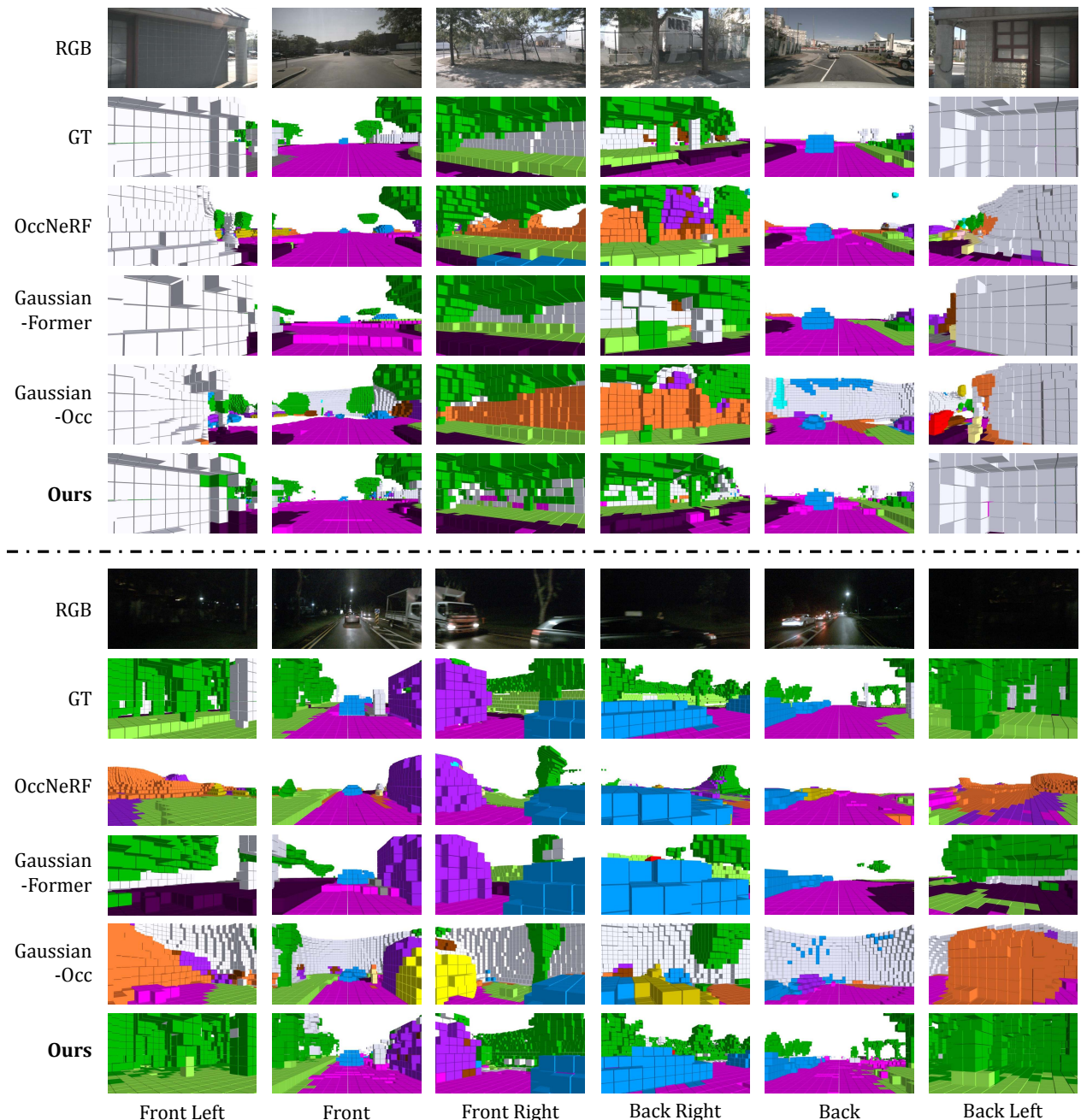


Figure 8. **Qualitative results of semantic occupancy reconstruction on Occ3D-nuScenes [50].** Our method enables efficient and accurate reconstruction of semantic 3D occupancy in dynamic objects and complex scene structures, even under extreme weather conditions.

for all scenes. For cross-dataset zero-shot occupancy estimation on SemanticKITTI [1], we use the specified range of [0.0m, -25.6m, -2.0m, 51.2m, 25.6m, 4.4m] with a voxel size of 0.2m. In contrast to [14, 37, 66], we do not require additional depth supervision or depth optimization, as LiDAR provides relatively accurate depth priors for the Gaussians’ initialization. By directly integrating depth information from sparse LiDAR points into SGAG, we eliminate the need for 2D depth maps generated by corresponding point

clouds or representations [12, 17]. The semantic category with the highest probability γ is assigned as the semantic attribute of each Gaussian, and the scale of γ is dynamically learned and derived from the open-vocabulary semantic labels per pixel. During optimization, the semantic probability γ is continuously updated based on VLMs clues. For every 1,000 iterations, Gaussians with opacity $\alpha = 0$ are removed.

Table 6. **Comparison with Baselines.** Base, Dynamic, and Unseen represent the semantic occupancy estimation results on the seen base classes, dynamic object classes, and cross-dataset unseen classes, respectively. Training Time stands for the average GPU hours required to train each scene. All experiments are conducted under consistent configurations.

Method	Base (mIoU \uparrow)	Dynamic (mIoU \uparrow)	Unseen (mIoU \uparrow)	Training Time (h)	Inference Speed (ms)	Memory (G)
OccNeRF [66]	10.81	4.17	0.00	0.64	93	77.1
GaussianOcc [12]	11.26	7.94	0.00	0.18	95	32.7
OccGS-Z	30.26	22.31	7.15	0.04	82	4.8



Figure 9. **Qualitative results of cross-dataset zero-shot occupancy estimation on SemanticKITTI [1].** OccGS achieves high-quality zero-shot open-vocabulary occupancy estimation while preserving fine geometric details and accurate semantic categories.

B. Additional Results

Quantitative Comparisons on Occ3D-nuScenes. In Table 5, we present comparisons with recent works on Occ3D-nuScenes [50]. These approaches can be roughly classified into five types based on the modality and training strategy:

- Multimodal supervised methods [32, 35] take multimodal sensor data as input and use manually labeled 3D occupancy ground truth (GT) as supervision for training.
- Vision-centric supervised methods [4, 18, 25, 27, 28, 50, 56, 59, 68] use surrounding or monocular images paired with manually labeled 3D GT for supervised training.
- LiDAR-centric supervised methods [7, 59] take LiDAR data as input and use manually labeled 3D occupancy/LiDAR GT as supervision for training.
- Semi-supervised or self-supervised methods [14, 37] train using 2D annotations, which are derived from manually labeled 3D ground truth.
- Fully self-supervised methods [2, 12, 17, 66, 73] are

trained using raw images, with supervision from 2D pseudo-labels generated by pre-trained models. Among these, [2, 73] enables open-vocabulary estimation, while the others are closed-set occupancy estimation models.

We reproduce the methods under the corresponding experimental settings. Due to some works not being open-sourced, the results reported in the table are sourced from their publicly available papers.

In contrast to the aforementioned methods, we propose a reconstruction-based multimodal semantic occupancy estimation approach that does not rely on manually labeled 2D/3D GT or large-scale, data-intensive training. OccGS supports open-vocabulary semantics and zero-shot cross-dataset optimization, delivering faster speed with lower computational cost. Our method achieves competitive performance compared to multimodal and vision-centric supervised methods and performs favorably against semi-supervised algorithms using 2D ground truth and fully self-supervised approaches.

Table 7. **Ablation of LiDAR-guided Geometry.** Random sampling refers to randomly sampling points of the same scale, while SfM refers to the point cloud estimated by Structure-from-Motion.

Model	IoU \uparrow	mIoU \uparrow
Random Sampling	80.09	16.47
Ours (w/ SfM)	80.87	22.65
Ours (w/ LiDAR)	83.82	30.26

Qualitative Comparisons on Occ3D-nuScenes. We present additional qualitative comparisons with SOTA methods on the Occ3D-nuScenes [50] dataset. Figure 8 illustrates that our method outperforms the baselines in semantic accuracy, consistency, and geometric completeness. OccGS delivers favorable results for detailed regions and fine structures, closely matching or even surpassing the manually labeled ground truth, and shows strong robustness in challenging weather conditions, such as rain and night.

Qualitative Comparisons for Zero-shot Estimation on SemanticKITTI. To validate the open-vocabulary semantics and zero-shot cross-dataset learning capability, we qualitatively compare our method with the baselines [12, 18, 59, 66] on SemanticKITTI [1]. The baselines encounter challenges with cross-dataset data distributions, varying voxel resolutions, and unseen semantic categories, resulting in notable semantic errors, geometric distortions, and inconsistencies (Figure 9). In contrast, our method demonstrates robust generalization to cross-dataset scenes and open-vocabulary categories, achieving high-quality occupancy estimation with precise geometry and semantics.

Comparisons with Baseline Approaches. We comprehensively compare our method with baselines [12, 66] across several aspects, including performance, training and inference speed, and memory consumption (Table 6). Both approaches suffer from high optimization and storage costs. They also encounter difficulties in handling dynamic objects, which are essential for outdoor driving scenarios, and are limited in zero-shot open-vocabulary occupancy estimation, resulting in less favorable performance on unseen categories. In comparison, our method achieves a good trade-off between performance and efficiency, delivering higher training and inference speeds with better accuracy.

C. Additional Ablation Studies

2D Semantics from VLMs. 2D ground truth, derived from manually annotated 3D data, is generated by projecting labeled 3D occupancy or LiDAR points onto 2D images and assigning semantic labels to each pixel. We project the semantics extracted by VLMs and the 3D annotated GT onto 2D images to assess the quality of the semantics extracted by VLMs against the 2D GT. The results show that VLM-extracted 2D semantics achieve a mIoU of 35.52 with the 2D GT and an IoU of 79.40. OccGS further enhances 3D semantic accuracy and consistency by leveraging multi-view

Table 8. **Ablation of hyperparameters.** ρ refers to the dynamic threshold for dynamic objects clustering.

ρ	IoU \uparrow	mIoU \uparrow
1	83.79	29.82
2	83.84	30.05
3	83.80	30.17
4	83.82	30.26
5	83.80	30.22
6	83.78	30.20
7	83.81	30.23

and multimodal semantic alignment to construct a unified 3D Gaussian representation.

Comparisons between OccGS-Z and OccGS-S. OccGS-Z does not require any manual annotations, while OccGS-S uses 2D GT derived from manually annotated 3D data. Table 5 shows that OccGS-S performs favorably against OccGS-Z in mIoU, benefiting from the more accurate 2D semantic GT. Conversely, OccGS-Z slightly outperforms OccGS-S in terms of IoU, suggesting that while more accurate 2D GT improves semantic occupancy estimation, it may limit the reconstruction of occupancy (0-1) geometry.

LiDAR-guided Geometry Prior for Initialization. To validate the effectiveness of the LiDAR-guided geometry prior, we conduct an ablation study by replacing LiDAR with randomly sampled points and point clouds estimated by Structure-from-Motion (SfM) [43, 45]. Table 7 demonstrates the effectiveness of LiDAR in enhancing semantic structures, outperforming both randomly sampled points and point clouds estimated by SfM. The experimental results also show that our method performs excellently even without using Lidar point priors, relying solely on visual images as input. OccGS supports both visual and multimodal data and demonstrates good generalizability.

Hyperparameter Analysis. We conduct an ablation study on the hyperparameter ρ , which represents the threshold for dynamic objects clustering. In the other main experiments, we set ρ to 4. Table 8 presents the performance evaluation under different hyperparameter settings. Our method demonstrates strong robustness to hyperparameters, making it applicable to varied unseen scenes.

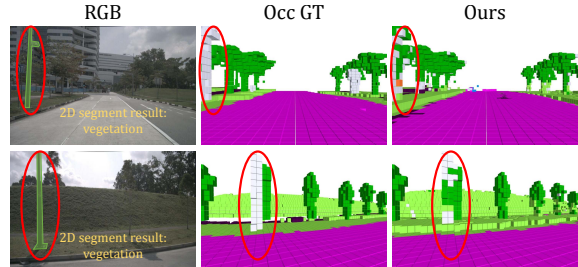


Figure 10. **Failure Cases.** The main limitation of our method stems from the ambiguity and missing regions present in the 2D semantics extracted by VLMs.

D. Failure Cases and Limitations

The main limitation of our method lies in the accuracy and completeness of semantic extraction by VLMs in open-world scenarios. Figure 10 shows that for erroneous semantic extraction by VLMs, our method is unable to fully rectify these errors, leading to semantic ambiguity in certain geometric regions. Future work will focus on incorporating more advanced VLMs to improve semantic knowledge transfer in semantic 3D occupancy estimation.

Broader Impacts

This paper presents research aimed at advancing the fields of 3D vision and autonomous driving, which hold significant promise for enhancing the capabilities of autonomous systems. While AI-driven scene reconstruction and perception bring benefits, they could also raise concerns regarding their social and economic impacts. Automating 3D labeling and perception tasks can potentially disrupt the labor market, posing risks to certain job sectors, particularly in sectors that rely on manual data annotation. It is crucial to exercise caution and ensure that the societal implications are thoroughly addressed.